Physica B 480 (2016) 116–124

Contents lists available at ScienceDirect

Physica B

journal homepage: www.elsevier.com/locate/physb

Structural and luminescence properties of $SrAl_2O_4:Eu^{2+},Dy^{3+},Nd^{3+}$ phosphor thin films grown by pulsed laser deposition

A.H. Wako [a,*], F.B. Dejene [a], H.C. Swart [b]

[a] Department of Physics, University of the Free State, QwaQwa Campus, Private Bag X13, Phuthaditjhaba 9866, South Africa
[b] Department of Physics, University of the Free State, P.O. Box 339, Bloemfontein ZA-9300, South Africa

ARTICLE INFO

Article history:
Received 7 May 2015
Received in revised form
22 September 2015
Accepted 27 September 2015
Available online 30 September 2015

Keywords:
Solution-combustion
$SrAl_2O_4:Eu^{2+},Dy^{3+},Nd^{3+}$
Thin films
Sr/Al mol%
Argon
Photoluminescence

ABSTRACT

Thin films of Eu^{2+} doped and Dy^{3+},Nd^{3+} co-doped Strontium Aluminate ($SrAl_2O_4:Eu^{2+},Dy^{3+},Nd^{3+}$) phosphors were grown on Si(100) substrates by a pulsed laser deposition (PLD) technique using a 266 nm Nd:YAG pulsed laser under varying substrate temperature and the working atmosphere during the film deposition process. The effect of substrate temperatures and argon partial pressure on the structure and luminescence properties of the as-deposited $SrAl_2O_4:Eu^{2+},Dy^{3+},Nd^{3+}$ phosphor thin films were analysed. XRD patterns showed that with increasing substrate temperature and argon partial pressure the peaks in the direction (220) shifted to the lower 2-theta angles. Photoluminescence (PL) data collected in air at room temperature revealed a slight shift in the peak wavelength of the PL spectra observed from the thin films when compared to the PL spectra of the phosphor in powder form, which is probably due to a change in the crystal field. The PL intensity of the samples was highest for 100 °C substrate temperature and 20 mTorr argon partial pressure. Due to this, the effect of argon partial pressure was studied at a constant substrate temperature of 100 °C while the effect of Substrate temperatures recorded at 20 mTorr argon pressure respectively.

1. Introduction

Long afterglow or persistent phosphors have the ability of absorbing energy from UV or sunlight and then release it slowly in the dark [1,2]. Inorganic phosphors doped with rare earth elements show broad band emission from blue to red which makes them suitable for a variety of industrial applications, such as luminescent pigments, fluorescent lamps, color display, plasma display panels (PDP), radiation dosimetry and X-ray imaging [3]. The type and duration of emission from a phosphor is affected by a number of parameters such as the type and amount of activators or dopants, the structure of the host lattice, the method of preparation or growth conditions and other post-treatments. These parameters play a significant role in inducing a crystal field effect within the host matrix which in turn influences the emission wavelength, its intensity and lifetime. The main task would therefore be to optimize these factors so at to obtain a phosphor that gives the best performance for the desired application.

Luminescent Eu^{2+}-doped strontium aluminate ($SrAl_2O_4:Eu^{2+}$) phosphors have been studied extensively because they exhibit excellent properties such as bright and long-persistent phosphorescence which glow for many hours and are also safer and chemically stable and free from radioactive radiations as compared with sulfide phosphors like ZnS:Cu [4]. Persistent luminescence and intensity can be enhanced by co-doping $SrAl_2O_4:Eu^{2+}$ with other rare earth elements [5]. Most of the research mainly focused on the trivalent dysprosium (Dy^{3+}) and not Neodymium (Nd^{3+}) ions as co-dopants. $SrAl_2O_4:Eu^{2+},Dy^{3+},Nd^{3+}$ phosphor powder can be synthesized using methods such as co-precipitation [6], solid state reaction [2] and sol–gel [7]. As compared with these conventional methods, solution-combustion synthesis technique [3–5] used in this work to prepare $SrAl_2O_4:Eu^{2+},Dy^{3+},Nd^{3+}$ phosphor powders is facile, energy saving, safe and fast [8].

Most of the previous studies on $SrAl_2O_4:Eu^{2+}$ were carried out on the phosphor powder and there are few reports on thin films more so those made using the PLD technique [9]. In this paper we report the structural and luminescence properties of as–prepared $SrAl_2O_4:Eu^{2+},Dy^{3+},Nd^{3+}$ phosphor powder and thin films. Thin film phosphors have several advantages over powders in that they exhibit better thermal stability, better adhesion to the substrate, higher lateral resolution and less out gassing in device applications [10]. Several methods have been used to grow thin films such as Chemical Bath Deposition (CBD) [11], rf magnetron sputtering [12], pulsed laser deposition (PLD) [13] and epoxide-catalyzed sol–gel methods [14]. However PLD has several advantages over other

* Corresponding author.
E-mail address: wakoah@ufs.ac.za (A.H. Wako).

http://dx.doi.org/10.1016/j.physb.2015.09.049
0921-4526/

techniques such as the homogeneous stoichiometric deposition of the ejected particles on to the substrate [15] and good quality thin films can be obtained at low temperatures [16] by varying parameters such as substrate distance, atmosphere and substrate temperature among others. These parameters affect thickness, roughness and overall quality of the obtained films which in turn influence the host structure, inducing crystal field and hence photoluminescence (PL) properties of $SrAl_2O_4:Eu^{2+},Dy^{3+},Nd^{3+}$. In this study thin films of $SrAl_2O_4:Eu^{2+},Dy^{3+},Nd^{3+}$ were prepared using PLD. The effect of varying argon gas pressure and substrate temperatures on the structure and photoluminescent (PL) properties of the $SrAl_2O_4:Eu^{2+},Dy^{3+},Nd^{3+}$ thin films were investigated.

2. Experimental

2.1. Synthesis

Stoichiometric amounts of analytical pure grade (Sigma-Aldrich, 99.9%) Sr $(NO_3)_2$, $Al(NO_3)_3 \cdot 9H_2O$, $Eu(NO_3)_3 \cdot 5H_2O$, $Dy(NO_3)_3$, $Nd(NO_3)_3$ and urea $(CO(NH_2)_2)$ were taken to prepare polycrystalline $SrAl_2O_4:Eu^{2+},Dy^{3+},Nd^{3+}$ phosphor via a solution-combustion method where the metal nitrates and urea were used as reactants and fuel, respectively. All the precursors were pulverized in agate mortar to obtain better homogeneity before being dissolved in the smallest possible amount of 10 ml of de-ionized water and thoroughly mixed using a magnetic stirrer for 15 min without heating to obtain a uniform aqueous solution. The nominal concentration was maintained at 1:0.035 mol% for Eu^{2+}:Dy^{3+} and 1:0.015 mol% for Eu^{2+}:Ndy^{3+} while that of Sr to Al was 1 mol%:2 mol% in all samples respectively. The optimum concentration was calculated to give a final composition of $SrAl_2O_4:Eu^{2+},Dy^{3+},Nd^{3+}$.

The solutions were then poured into China crucibles and placed one at a time in a muffle furnace pre-heated to 500 °C. The mixture ignited and a fast, self-sustaining combustion reaction took place. At first, the solution boiled losing all the water in the form of steam followed by decomposition letting off large amounts of gases (oxides of carbon, nitrogen and ammonia). The mixture then frothed and swelled enormously in to foam, followed by spontaneous ignition and smoldering which gradually led to an explosion rupturing the foam with a flame that glowed to incandescence. The product of combustion was a voluminous white dry $SrAl_2O_4:Eu^{2+},Dy^{3+},Nd^{3+}$ foam. The foam was taken out of the muffle furnace, cooled then milled resulting in a dry, and usually crystalline, fine white oxide powders. The whole combustion process took about 5 min. The powders were then stored in transparent glass sample bottles for characterization and PLD.

The $SrAl_2O_4:Eu^{2+},Dy^{3+},Nd^{3+}$ powder was then pressed into a pellet and used as a target for laser deposition after initial characterization. The pellet was heated at 200 °C for 2 h in an oven to expel moisture that may be present and make it hard and strong for use as a target for laser ablation. The pellet was not sintered at higher temperatures to avoid causing changes to the certain properties of the material and hence maintain the initial properties of the powder from which it was formed. However the low temperature could be the reason for the high density droplets formed on the surface of the deposited films, The target was then loaded on to a rotatable carousel inside the PLD chamber. The carousel rasters and rotates the target to prevent constant ablation by the laser beam from the same spot on the target. Silicon (100) wafers of approximately 1 cm^2 were used as substrates. The wafers were first cleaned in ultrasonic bath of acetone, ethanol and distilled water in that sequence then blow-dried with clean dry N_2 gas and placed on a fixed substrate holder in the PLD chamber parallel to the target at a distance of 4.5 cm. The chamber was then pumped down to vacuum of about 3.0×10^{-6} mbar. The target was first ablated in vacuum and then under varying argon working atmosphere of 10 mTorr, 20 mTorr and 30 mTorr each for 60 min at a constant substrate temperature of 100 °C and again ablated under varying substrate temperatures of 100, 200 and 300 °C at a constant 20 mtorr argon partial pressure respectively using a 266 nm Nd:YAG nanosecond (ns) pulsed laser with energy and frequency fixed at 45mJ/pulse (fluence of 0.2 J cm^{-2}) and 10 Hz, respectively. Low laser fluence is one way for reducing particulate formation on the deposited films[17].

2.2. Characterization

The structural composition of the $SrAl_2O_4:Eu^{2+},Dy^{3+},Nd^{3+}$ phosphor powder and thin films were determined using a Bruker-AXS D8 Advance X-ray diffractometer (Bruker Corporation of Germany) operating at 40 kV and 40 mA using Cu Kα=0.15406 nm from 15° to 65° (2θ), with a scan rate of 0.39° (2θ)/min and step scans with a step time of 152 s and step size of 0.02°(2θ). The morphologies of the phosphor powders and films were obtained using a JSM-7800F field emission Scanning Electron Microscope (SEM) coupled with an Energy Dispersive X-ray Spectrometer (EDS) for analysis of elemental composition and mapping while the surface topography and roughness were examined in contact mode using a Shimadzu SPM-9600 atomic force microscopy (AFM) with an in-built commercial software for calculating the root mean square (rms) values which indicates roughness of the films. The (PL) spectra were recorded at room temperature using a 325 nm He–Cd Laser. Reflectance (UV–vis) characteristics were measured in the range 200–700 nm using a Perkin Elmer Scan-Lambda 950 UV–vis spectrophotometer using 319 nm excitation lamp and a 860 nm monochromator with a slit width of 2.0 nm and scan speed of 141 nm/min and step size of 0.5 nm to select a single frequency (wavelength) from all of those provided by the lamp source and to scan over a desired frequency range.

3. Results and discussions

3.1. Structure and morphology analysis

XRD patterns of the $SrAl_2O_4:Eu^{2+},Dy^{3+},Nd^{3+}$ phosphor powder and thin films deposited in vacuum, 10, 20 and 30 mTorr argon and at 100, 200 and 300 °C substrate temperatures for 60 min, are shown in Fig. 1(a) and (b) respectively. The peaks fitted well with the powder and the JCPDS card number 74-0794 for the monoclinic $SrAl_2O_4$ of space group P1211 (4), cell ratios $a/b=0.9581$ $b/c=1.7075$ $c/a=0.6112$ and cell parameters; $a=8.4470$ Å, $b=8.8160$ Å, $c=5.1630$ Å and $\beta=93.42°$. A peak representing $SrAl_4O_7$ phase was also detected as indicated by * which could be due to a small percentage change during the synthesis stage of the powder samples. Fig. 1(c) and (d) shows log of XRD Intensity vs. argon pressure and substrate temperature. It is observed that the intensities increase exponentially with argon pressure and substrate temperature respectively. It can be seen in Fig. 2(a) that with increasing argon pressure the peaks in the direction (220) shifted to the lower 2-theta angles from 29.1° in vacuum to 27.9° in 30 mTorr argon pressure accompanied by width-narrowing and increased intensity, an indication of increasing particle size as displayed in Fig. 2(b).

The average crystallite sizes calculated for the (220) direction were obtained using Scherrer's equation $D=K\lambda/(\beta\cos\theta)$ where D is the mean particle size, K is a geometric factor, λ is the X-ray wavelength and β is Full With at Half Maximum (FWHM). The same trend was observed when substrate temperature was varied

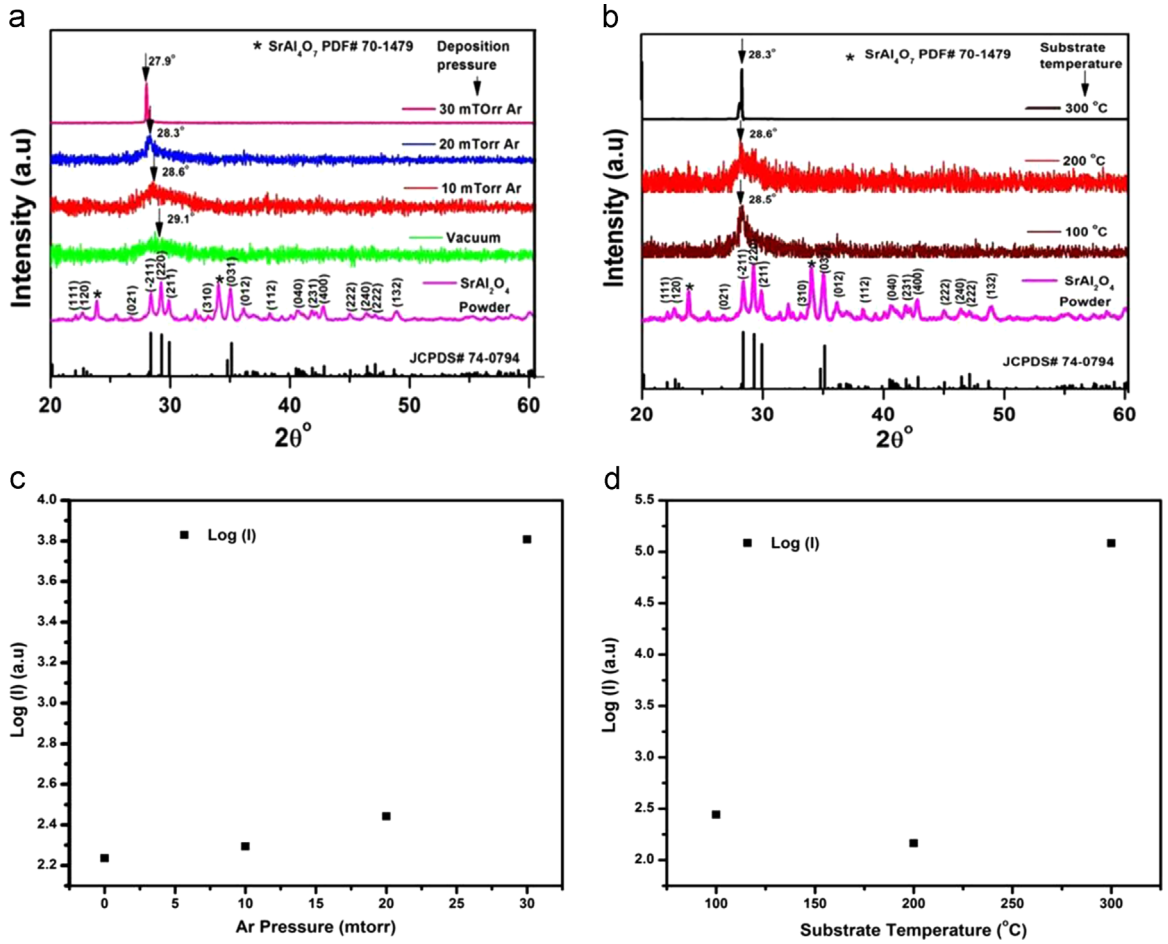

Fig. 1. XRD patterns of the $SrAl_2O_4$:Eu^{2+},Dy^{3+},Nd^{3+} phosphor powder ($SrAl_2O_4$) and thin films that were deposited in (a) Vacuum, 10, 20 and 30 mTorr argon, (b) at 100, 200 and 300 °C substrate temperature for 60 min and log (intensity) plots for vacuum-argon pressures (c) and aubstrate tempratures (d).

as seen in Figs. 1(b), 2(c) and 2(d). With increasing substrate temperature, the peaks in the direction (220) shifted to the lower angle from 28.5° at 100 °C to 28.3° at 300 °C accompanied by width-narrowing and increased intensity, an indication of increasing particle size as displayed in Fig. 2(b).

Broad XRD peaks is an indication of decreasing particle size, beginning of crystallization and short-range ordering [18] while the reverse case would mean that the material is amorphous which can be observed from the XRD patterns. However the drastic increase of particle size at 300 °C is not that evident from the AFM images but SEM. Argon being a heavier gas scattered away more particles in the plume and this affected the arrival rates of all the species. Light atoms are scattered more than heavy atoms [19,20].

From Fig. 2(a)–(d) it was deduced that the XRD peak positions, FWHM, intensity and crystallite size were influenced by the ambient gas pressure and the variation of substrate temperature.

3D AFM images of the surface topography of the films deposited on Si (100) under different argon pressures are shown in Fig. 3(a)–(c) and those deposited under different substrate temperatures are shown in Fig. 3(d)–(f).

The films showed well defined and generally spherical grains of different sizes uniformly distributed over the surface which could be attributed to the reduced speed and hence arrival rates of the particles in the plume by the gas molecules thereby allowing a better nucleation process of the film particles on the substrate during the ablation process [21]. The AFM oscilloscope signal obtained from a section of the sample during the scanning of the surface topography the of $SrAl_2O_4$:Eu^{2+},Dy^{3+},Nd^{3+} thin films was shown in Fig. 3(g). It depicted the spherical shapes of the grains and revealed sections where the particles agglomerated and formed larger clusters. From the figure the average particle size estimated from the vertical *z*-axis was found to be 100 nm which is within the same range as those shown in Fig. 2 calculated using the Scherrer equation.

The variation of film roughness indicated by the root mean square (rms) or Rq values with argon pressure and substrate temperature were shown in Fig. 4(a) and (b) respectively.

It was observed that the film roughness increased with increasing argon pressure and decreased with increasing substrate temperature. A decrease in surface roughness with the increase in substrate temperature has also been reported elsewhere [9]. Also from Fig. 2 it is observed that the grain sizes increased as the ambient argon gas pressure increased. The reason for this is that when the gas pressure in the chamber is low the mean free path (MFP) of the particles is longer hence yielding less effective collisions, whereas as the gas pressure increases the MFP also increases resulting in more effective collisions between the particles leading to nucleation and growth resulting in bigger particles [21,22]. It was also reported elsewhere that background gas of Ar has a higher mass density and therefore tends to reflect lighter atoms in the plume more and these results in a film with big particles on the substrate [23].

The SEM micrograph, elemental map, and EDS energy distribution micrographs of $SrAl_2O_4$:Eu^{2+},Dy^{3+},Nd^{3+} thin films and $SrAl_2O_4$:Eu^{2+},Dy^{3+},Nd^{3+} powder are shown in Fig. 5(a)–(h). In the SEM micrograph, Fig. 5(a) it is clear that the thin films have larger particles on the surface. In the past these particles showed

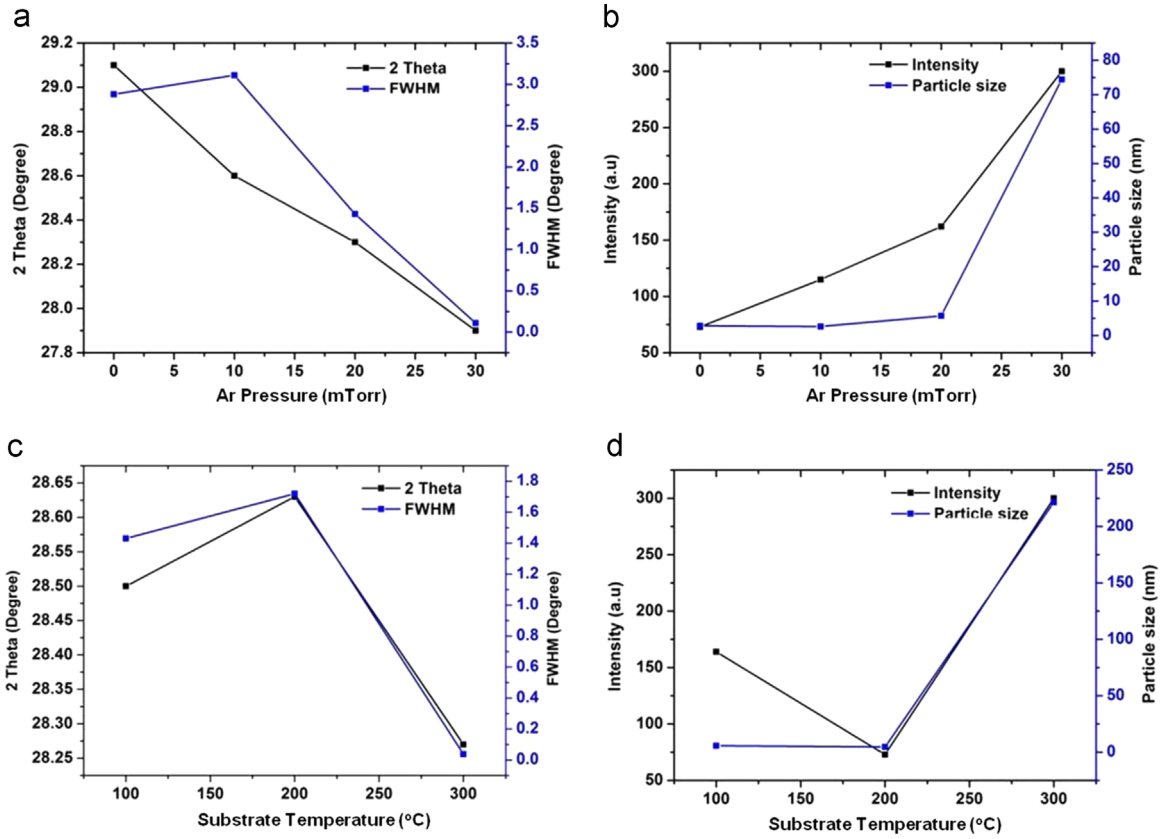

Fig. 2. 2theta, FWHM, particle size and intensity as a function of argon pressure; (a) and (b) and substrate temperature; (c) and (d).

more intense luminescence than the rest of the film due to less internal reflection [23].

Fig. 5(b) shows the relative compositional quantities of the individual elements in the sample. The EDS energy microanalysis was employed to approach elements' contribution in the sample. However the very low concentration of the rare earth dopants could be the reason for not being detected in the EDS spectra. Also Nd^{3+} was not detected at even in the SEM owing to the very low concentration as compared to Eu^{2+} and Dy^{3+}.

The 2D elemental maps revealing the coordination and distribution of the different species (Sr, Al, O and Dy) in the $SrAl_2O_4$ host nanophosphor at the nanoscale are shown in Fig. 5(c). It confirmed their elemental composition, locations and distributions within the $SrAl_2O_4$:Eu^{2+}, Dy^{3+} phosphor thin films. The EDS elemental mapping micro images of Si, Sr, Al, O, Dy and Eu in the films are also shown in Fig. 5(d)–(i). From the mapping images it seems that the bigger particles were slightly enriched with Al and O with respect to the rest of the thin film and as such Fig. 5(e) and (f) droplets seem to contain more Al, O and less Sr in accordance with the relative chemical composition $SrAl_2O_4$. The rest of the elements were uniformly distributed in the thin films.

3.2. Photoluminescence

PL emission spectra recorded with the He–Cd laser at an excitation of 325 nm from the $SrAl_2O_4$:Eu^{2+},Dy^{3+},Nd^{3+} as prepared powder and $SrAl_2O_4$:Eu^{2+},Dy^{3+},Nd^{3+} thin films deposited on Si (100) under different argon pressures and substrate temperatures respectively was shown in Fig. 6.

Fig. 6(a) represents the $SrAl_2O_4$:Eu^{2+},Dy^{3+},Nd^{3+} phosphor powder which yielded a bright green luminescence emission peaking at 507 nm resulting from transitions between the $4f^6 5d^1$–$4f^7$ electron configurations of Eu^{2+} with only one emission broad band which is symmetric, an indication that only one luminescent centre, which is Eu^{2+}exists [5]. The effect of the varied chamber parameters was observed as shown in Fig. 6(b) and (c) whereby emission peaks are shifted to the longer wavelength side as also seen in Fig. 6(d). In RE ions the $4f^n$ electron shell is shielded from outside by 5s and 5p electrons thereby screening them from surrounding crystal field effects hence Nd^{3+} acts as traps of holes and the trap level lie in between the excited and ground states of Eu^{2+} which enhances luminescence [24]. The slight wavelength shift could therefore be attributed to the different deposition conditions of argon pressure and substrate temperatures which induced crystal field effect within the $SrAl_2O_4$ host lattice.

The PL intensities of the films are generally low compared to those of the powder due to total internal reflection in thin films [25]. However thin films have advantages over the powders in that they possess better thermal stability, better adhesion to the substrate, higher lateral resolution and less out gassing in device applications [10,26].

The shift in the PL emission peaks of Fig. 6 is clearly seen on the CIE color chromatography plots of Fig. 7(a) and (b) depicting color shifts with respect to changes in argon partial pressure and substrate temperature respectively. As indicated by the arrows it is clear that as the argon gas pressure varies from 10 to 30 mTorr and substrate temperature from 100 to 300 °C, the CIE co-ordinates shift toward the longer wavelength of the CIE map.

3.3. UV–vis analysis

Fig. 8(a) and (b) also shows how the UV-reflectance is affected by the deposition atmospheres of argon and substrate temperature. It was observed that reflectance decreased with increase in the gas pressure and substrate temperature. Also the absorption

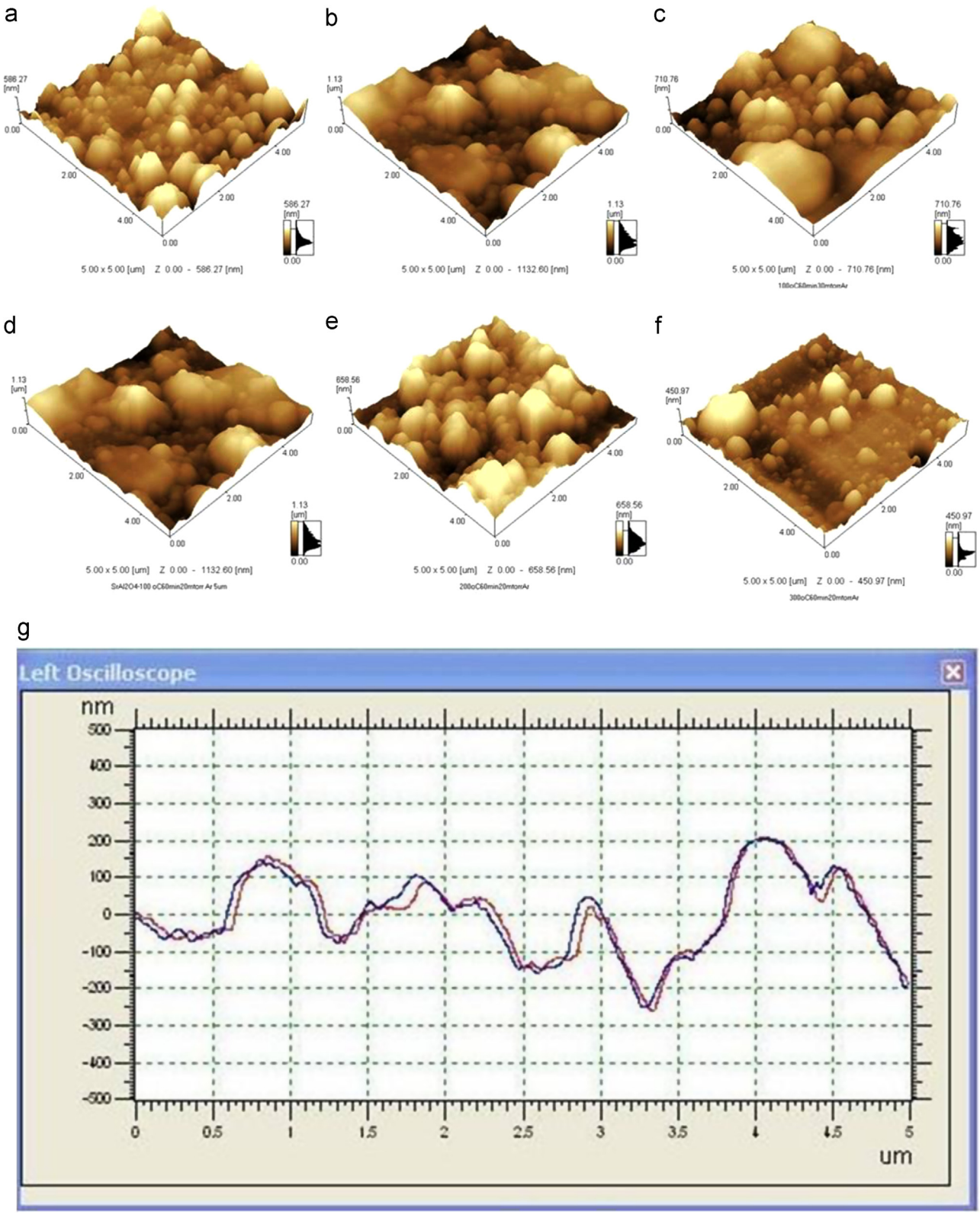

Fig. 3. 3D AFM images of $SrAl_2O_4$:Eu^{2+},Dy^{3+},Nd^{3+} thin films deposited in (a) 10 mTorr, (b) 20 mTorr (c) 30 mTorr argon pressures; (d) 100 °C (e) 200 °C, (f) 300 °C substrate temperatures; and (g) AFM oscilloscope showing surface topography profile of $SrAl_2O_4$:Eu^{2+},Dy^{3+},Nd^{3+} thin films.

edges of the different spectra varied according to the different PLD chamber environment. This could be explained in the same way as the PL wavelength shifts attributed to the crystal field effect due to changes in the host structure.

The average band gap energies were obtained from the intercept of the extrapolated linear portion from of the $(f(\boldsymbol{R}(v)hv)^n$ vs. hv plot known as Tauc's plot along the hv axis as shown in Fig. 8(c) and (d) for vacuum, 10, 20 and 30 mTorr Ar and substrate temperature respectively. It revealed that absorption was greatly influenced by the presence of a background gas. The band gap

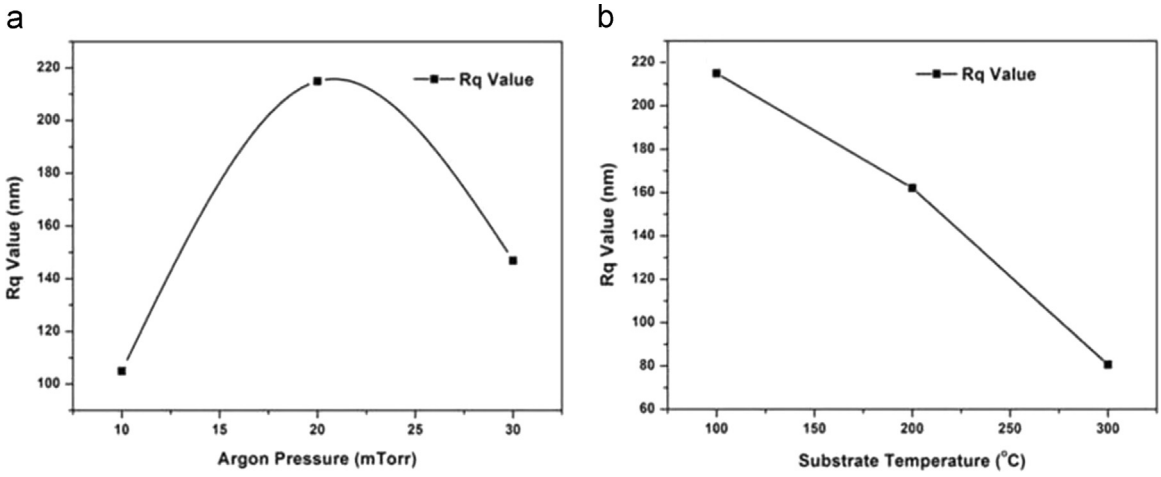

Fig. 4. Variation of film roughness (Rq value) with (a) argon pressure and (b) substrate temperature.

energy reduced as the amount of ambient gas increased (Fig. 8(c)) and increased with increasing substrate temperature (Fig. 8(d)). This energy gap shift corresponds with the shifts observed in Fig. 6 (d). Since Energy is inversely proportional to the wavelength ($E_g \propto \frac{1}{\lambda}$), as the wavelength increased the band gap decreased. Also as the wavelength shifted towards the longer side the band

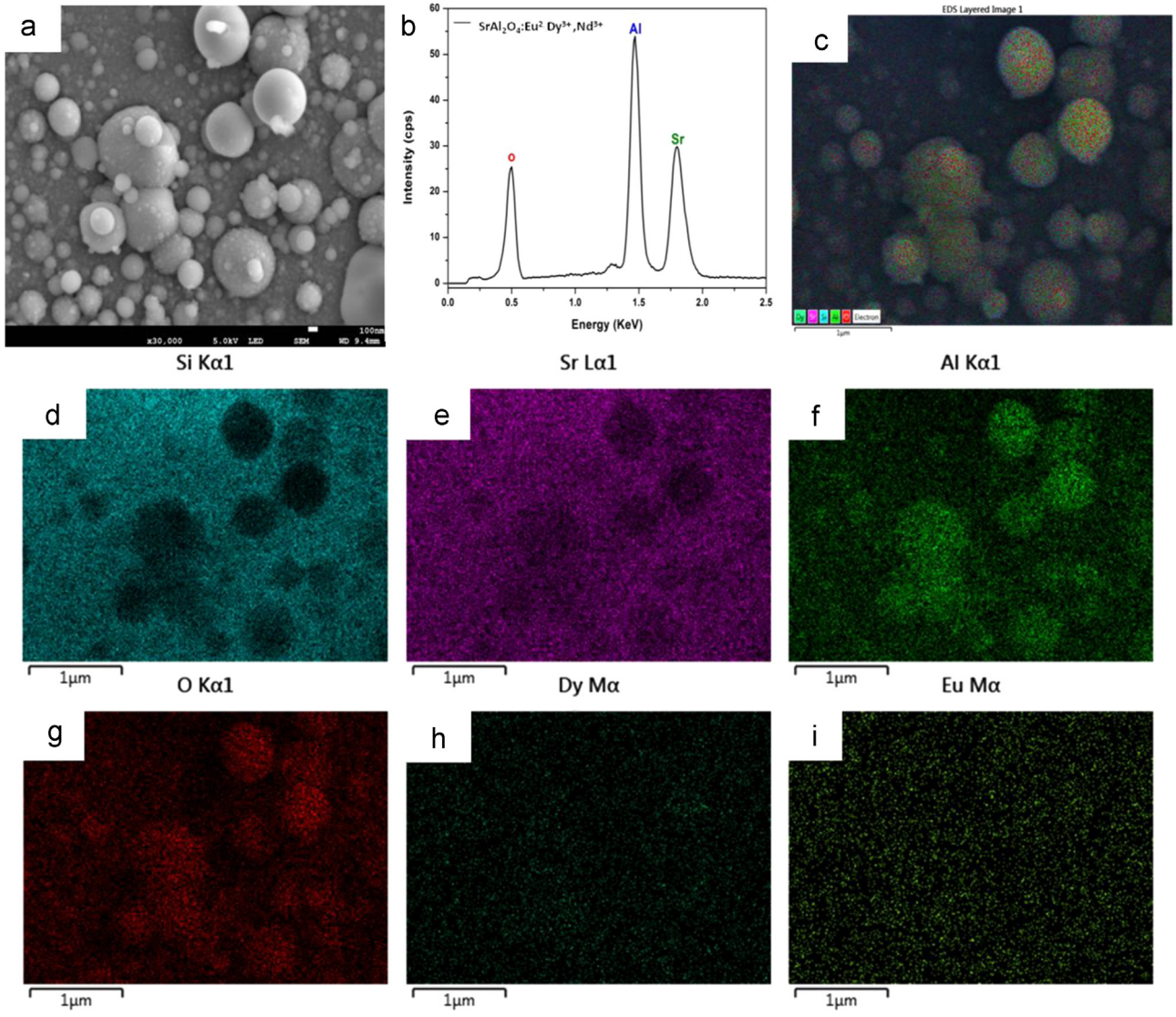

Fig. 5. (a) SEM micrograph, (b) EDS profile, (c) Elemental map (d) SiKα1 (e) SrLα1 (f) AlKα1 (g) OKα1, (h) DyMα and (i) EuM α energy distributions of $SrAl_2O_4$:Eu^{2+},Dy^{3+},Nd^{3+} thin films.

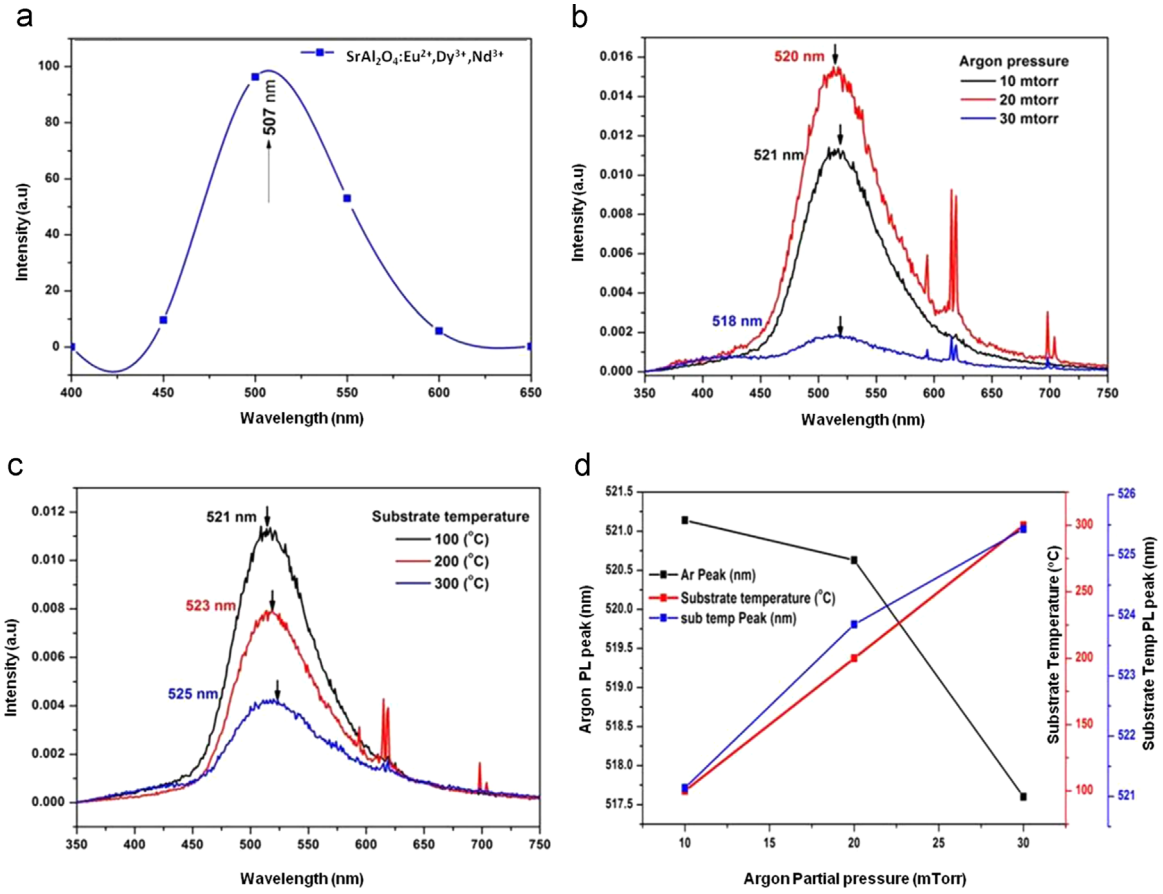

Fig. 6. Emission spectra for (a) $SrAl_2O_4:Eu^{2+},Dy^{3+},Nd^{3+}$ phosphor powders, (b) $SrAl_2O_4:Eu^{2+},Dy^{3+},Nd^{3+}$ thin flms variation with argon pressure,(c) $SrAl_2O_4:Eu^{2+},Dy^{3+},Nd^{3+}$ thin films variation with substrate temperature and (d) Comparison of emission peak shifts due to argon partial pressure (black) and substrate temperature (blue) as a function of argon partial pressure and substrate temperature (red) for $SrAl_2O_4:Eu^{2+},Dy^{3+},Nd^{3+}$ thin films. (For interpretation of the references to color in this figure legend, the reader is referred to the web version of this article.)

gap is reduced. Narrow band gap materials exhibit novel properties such as small effective masses, improved surface and interface properties and the possibility of incorporating more impurity/dopant ions [27].

4. Conclusion

In this study thin films of $SrAl_2O_4:Eu^{2+},Dy^{3+},Nd^{3+}$were prepared using the PLD technique. The effect of varied background gas

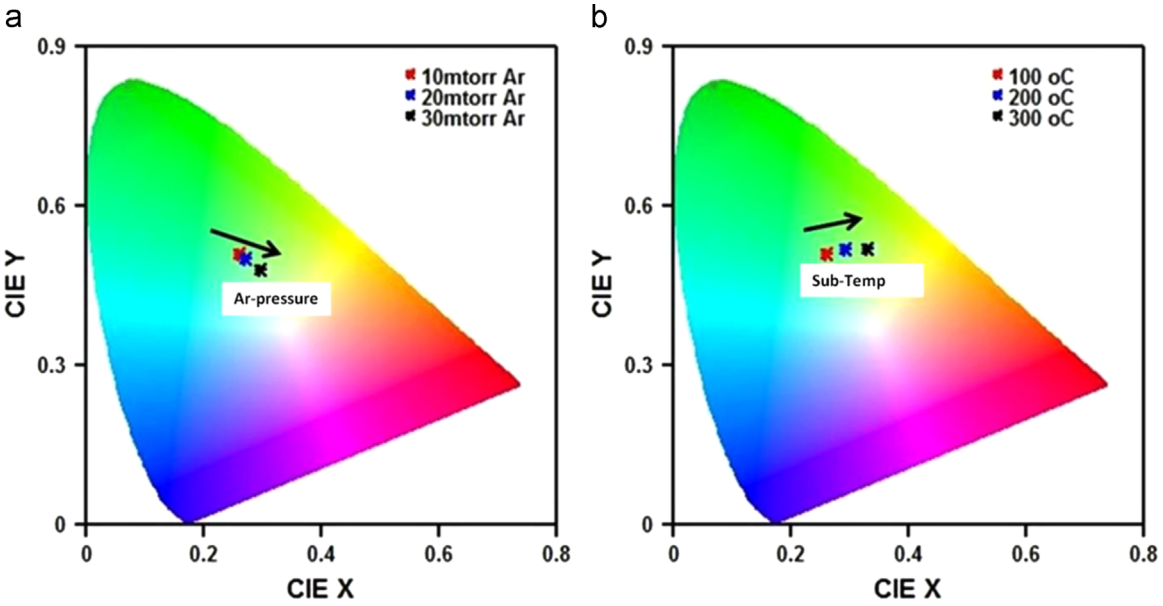

Fig. 7. Chromaticity diagram depicting CIE color co-ordinates with respect to the changes in (a) the argon atmosphere and (b)substrate temperature during ablation. (For interpretation of the references to color in this figure, the reader is referred to the web version of this article.)

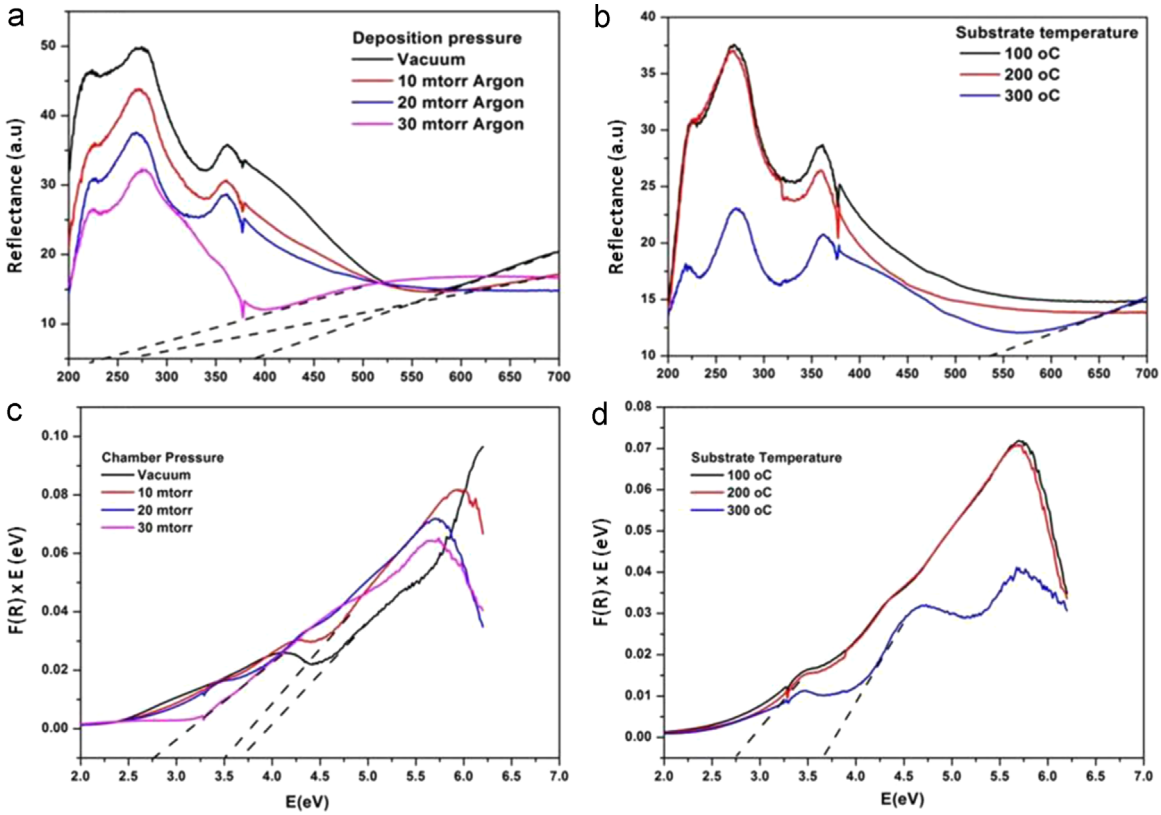

Fig. 8. (a)–(d) UV–vis reflectance and Tauc's plot as per the deposition atmospheres of argon and substrate temperature.

pressure and substrate temperature on the structure and PL properties of the $SrAl_2O_4:Eu^{2+},Dy^{3+},Nd^{3+}$ thin films were investigated. It was found that with increasing argon pressure and substrate temperature the peaks in the direction (220) shifted to the lower angle accompanied by width-narrowing and increased intensity an indication of increasing particle size. Also the film roughness increased with increasing argon pressure and decreased with increasing substrate temperature. The emission peaks were observed to shift to the longer wavelength side which could be attributed to the different deposition conditions of argon partial pressure and substrate temperatures which induced crystal field effect within the $SrAl_2O_4$ host lattice. The reflectance intensity decreased with increasing gas pressure and substrate temperature.

Acknowledgment

The authors acknowledge with immense gratitude the South African National Laser Centre (NLC) and the Council for Scientific and Industrial Research (CSIR) for assisting with the PLD technique for film ablation and deposition and also for technical, financial and logistical support during research visits to the NLC labs. This work is based on the research supported by the South African Research Chairs Initiative (Grant no. 84415) of the Department of Science and Technology, and the National Research Foundation of South Africa and University of the Free State Cluster Fund.

References

[1] S. Nagamani, B.S. Panighrahi, Luminescence properties of SrO–Al_2O_3:Eu^{2+}, Dy^{3+} prepared at different temperatures, J. Am. Ceram. Soc. 93 (2010) 3832–3836.
[2] P. Taylor, X. Duan, S. Huang, F. You, Z. Xu, Electrooptical characteristics of nanoscale and bulk long persistent phosphor $SrAl_2O_4$:Eu, Dy, J. Exp. Nanosci. 4 (2009) 169–176.
[3] V. Singh, J. Zhu, V. Natarajan, Eu^{2+} and Sm^{3+} emission in $SrAl_{12}O_{19}$ phosphors prepared via combustion synthesis, Phys. Status Solidi 203 (2006) 2058–2064.
[4] N.M. Son, L.T.T. Vien, L.V.K. Bao, N.N. Trac, Synthesis of $SrAl_2O_4:Eu^{2+},Dy^{3+}$ phosphorescence nanosized powder by combustion method and its optical properties, J. Phys. 187 (012017) (2009) 1–6.
[5] T. Peng, H. Yang, X. Pu, B. Hu, Z. Jiang, C. Yan, Combustion synthesis and photoluminescence of $SrAl_2O_4$:Eu, Dy phosphor nanoparticles, Mater. Lett. 58 (2004) 352–356.
[6] S. Choi, N. Kim, Y. Yun, S. Choi, phosphors synthesized by an oxalate coprecipitation method, J. Ceram. Process. Res. 7 (2006) 62–65.
[7] P. Huang, C.-E. Cui, S. Wang, Synthesis and characterization of $Sr_3Al_2O_6:Eu^{2+}$, Dy^{3+} phosphors prepared by sol–gel–combustion processing, Chin. Phys. B 18 (2009) 4524–4531.
[8] A.H. Wako, B.F. Dejene, H.C. Swart, Roles of doping ions in afterglow properties of blue $CaAl_2O_4:Eu^{2+},Nd^{3+}$ phosphors, Phys. B Condens. Matter 439 (2014) 153–159.
[9] P.D. Nsimama, O.M. Ntwaeaborwa, E. Coetsee, H.C. Swart, The influence of the number of pulses on the morphological and photoluminescence properties of $SrAl_2O_4:Eu^{2+},Dy^{3+}$ thin films prepared by pulsed laser deposition, Phys. B Condens. Matter 404 (2009) 4489–4492.
[10] K.T. Hillie, O.M. Ntweaeborwa, H.C. Swart, Degradation of pulse laser deposited Y_2O_3:Eu thin film phosphor, Phys. Status Solidi 1 (2004) 2360–2365.
[11] L.F. Koao, F.B. Dejene, H.C. Swart, Properties of flower-like ZnO nanostructures synthesized using the chemical bath deposition, Mater. Sci. Semicond. Process. 27 (2014) 33–40.
[12] Y. Deng, J.D. Fowlkes, P.D. Rack, J.M. Fitz-Gerald, Thin film rf magnetron sputtering of gadolinium-doped yttrium aluminum garnet ultraviolet emitting materials, Opt. Mater. 29 (2006) 183–191.
[13] A. Yousif, H.C. Swart, J.J. Terblans, R.M. Jafer, V. Kumar, R.E. Kroon, O. M. Ntwaeaborwa, M.M. Duvenhage, Structural and morphology analysis of annealed $Y_3(Al,Ga)_5O_{12}$:Tb thin films synthesized by pulsed laser deposition, Appl. Surf. Sci. 305 (2014) 732–739.
[14] S. Murai, M.A. Verschuuren, G. Lozano, G. Pirruccio, A.F. Koenderink, J.G. Rivas, Enhanced absorption and emission of $Y_3Al_5O_{12}:Ce^{3+}$ thin layers prepared by epoxide-catalyzed sol–gel method, Opt. Soc. Am. 2 (2012) 1707–1715.
[15] J. Lancok, C. Garapon, V. Vorlíček, M. Jelinek, M. Čerňanský, Structural and fluorescence properties of thin films fabricated by pulsed laser deposition technique from Nd:KGW single crystal, Opt. Mater. 28 (2006) 360–369.
[16] X.W. Sun, H.S. Kwok, Pulsed laser deposition of silicate phosphor thin films, Appl. Phys. A 69 (1999) S39–S43.
[17] M.N.R. Ashfold, F. Claeyssens, G.M. Fuge, S.J. Henley, Pulsed laser ablation and deposition of thin films, Chem. Soc. Rev. 33 (2004) 23–31.
[18] L.I.U. Chun-jia, Y.U. Rui-min, X.U. Zhi-wei, C.A.I. Jing, Y.A.N. Xing-huang, L.U.

O. Xue-tao, M. Science, C. Engineering, Crystallization, morphology and luminescent properties of YAG:Ce^{3+} phosphor powder prepared by polyacrylamide gel method, Trans. Nonferrous Met. Soc. China 17 (2007) 1093–1099.
[19] Y. Nakata, W.K.A. Kumuduni, T. Okada, M. Maeda, Plume-substrate interaction thin films in pulsed-laser deposition of high-temperature superconducting thin films, Appl. Phys. Lett. 2599 (2005) 1–4.
[20] J.M. Warrender, M.J. Aziz, Kinetic energy effects on morphology evolution during pulsed laser deposition of metal-on-insulator films, Phys. Rev. B 75 (2007) 1.
[21] P.D. Nsimama, The surface analysis and photoluminescence properties of $SrAl_2O_4:Eu^{2+},Dy^{3+}$ thin films prepared by the pulsed laser deposition technique, Tanzan. J. Appl. Sci. *2* (2011) 268–276.
[22] H.C. Swart, O.M. Ntwaeaborwa, P.D. Nsimama, J.J. Terblans, Surface characterization and luminescent properties of $SrAl_2O_4:Eu^{2+},Dy^{3+}$ nano thin films, Phys. B Condens. Matter 407 (2012) 1660–1663.
[23] S.T.S. Dlamini, H.C. Swart, J.J. Terblans, O.M. Ntwaeaborwa, The effect of different gas atmospheres on the structure, morphology and photoluminescence properties of pulsed laser deposited $Y_3(Al,Ga)_5O_{12}:Ce^{3+}$ nano thin films, Solid State Sci. 23 (2013) 65–71.
[24] H. Ryu, K.S. Bartwal, Photoluminescent spectra of Nd^{3+} codoped $CaAl_2O_4:Eu^{2+}$ blue phosphor, Res. Lett. Mater. Sci. 2007 (2007) 1–4.
[25] J. Choe, Luminescence and compositional analysis of $Y_3Al_5O_{12}$:Ce films fabricated by pulsed-laser deposition, Mater. Res Innov. 6 (2002) 238–241.
[26] A. Yousif, H.C. Swart, O.M. Ntwaeaborwa, E. Coetsee, Conversion of $Y_3(Al,Ga)_5O_{12}:Tb^{3+}$ to $Y_2Si_2O_7:Tb^{3+}$ thin film by annealing at higher temperatures, Appl. Surf. Sci. 270 (2013) 331–339.
[27] T.C. McGill, D. Collins, Prospects for the future of narrow bandgap materials, Semicond. Sci. Technol. 8 (1993) 1–5.